SUPPORTING INFORMATION

Ultrafast Photophysics of a Dinitrogen Bridged Molybdenum complex

Shahnawaz Rafiq, Máté J. Bezdek, Marius Koch, Paul J. Chirik*, Gregory D. Scholes*

Frick Chemistry Laboratory, Princeton University, NJ 08544

Email: gscholes@princeton.edu; pchirik@princeton.edu

Content

1. Sample Preparation for Spectroscopic Measurements

[1–N_2]$^{2+}$ and **1-Cl** are strongly air- and moisture-senstive metal complexes. Solutions of these metal complexes were prepared in an M. Braun inert atmosphere drybox containing an atmosphere of purified nitrogen. Solvents used in the spectroscopic measurements were dried and deoxygenated using literature procedures.[1] To avoid any possible traces of air- and moisture-degraded complex, samples were replenished between continuous measurements. Absorption spectra before and after the measurements were used as a reference to ensure that the sample has not degraded.

All spectroscopic measuements were performed in a 1 mm quartz cuvette fitted with a J-Young valve and sealed with a Teflon cap (shown below). The optical density of the samples was maintained around 0.4 in the cuvette. No traces of aggregation were observed at this concentration.

2. Experimental Methods

2.1 Steady-state Absorption Spectroscopy: Absorption spectra were recorded on a Cary 60 UV-Vis spectrophotometer (Agilent Technologies). Excitation slits 2/2 nm, emission slits 2/2. All the absorption spectra were measured in a 1mm path length quartz cuvette.

2.2 Transient Absorption Spectroscopy: Narrowband transient absorption measurements were performed on a commercial setup as described in reference.[2] Briefly, 40 fs, 800 nm laser light at a repetition rate of 1 kHz from a Ti:Sapphire regenerative amplifier (Libra, Coherent) was used to pump a commercial optical parametric amplifier (OPerA Solo, Coherent) to generate a narrowband pump pulses centered at 440, 520, 610, 730, and 1150 nm. A portion of the output from the OPA and a part of the fundamental output from the laser amplifier was directed to a commercial pump-probe spectrometer (Ultrafast Systems, Helios). The 800 nm output was focused into a sapphire plate to generate a white light continuum ranging from 430 – 750 nm in the visible region and 820 – 1600 nm in the near-infrared region. The time delay between the pump and probe was controlled by varying the travel time of the probe beam using a translation stage. The pump and the probe beams were focused into a sample cell of 1 mm path length.

2.3 Two-Dimensional Electronic Spectroscopy: The 2DES experimental setup is explained in detail elsewhere.[3-7] Briefly, 90 fs, 800 nm laser light at a repetition rate of 5 kHz from a Ti:sapphire seeded regenerative amplifier (Spectra-Physics, Spitfire) was used to pump a home-built non-collinear optical parametric amplifier (NOPA). The NOPA output was sent into a folded grating compressor and then into a two-prism compressor. The laser pulse was compressed to 12 fs for 2D electronic measurements as measured with polarization-gated and transient grating frequency-resolved optical grating (PG-, TG-FROG).[8-9] 2DES is a third-order non-linear optical spectroscopy technique which spreads the information contained in a typical pump-probe experiment into a frequency-frequency correlation map .[7, 10-11] Three incoming fields (E_1, E_2, E_3) interact with the sample in a particular phase-matching condition leading to the emission of a third order signal which is heterodyned detected by spectral interferometry with a fourth laser field, the local oscillator $E_{LO.}$ As such, both amplitude and phase information is retrieved. These four fields (E_1, E_2, E_3, and E_{LO}) were generated by focusing the compressed NOPA output on a 2D diffractive optic generating four phase-stable beams in a box-geometry. Three beams are passed through pairs of 1° fused silica wedges, each of which incorporates one mounted on a translation stage (Newport VP-25XL) to change the amount of glass a beam passes through. The third beam is passed through a chopper operating at 50 Hz to remove the scatter. The interaction of the first field with the sample creates a coherence between the ground and excited state which is clocked by the time period, τ, with respect to the second field. The second field onsets a population or another coherence and marks the beginning of the waiting time, t_2 and allows the system to evolve dynamically. The third pulse effectively ends the waiting time and marks the beginning of another coherence time, $t_{3,}$ and provides information about the instantaneous state of the system prepared by the interaction with the initial two pulses. The fourth beam acts as the local oscillator and is passed through a neutral density filter attenuating it by four orders of magnitude and imparting a delay such that it arrives ~250 fs before the final laser field. While the heterodyned detected signal is dispersed directly on the camera giving the detection axis (ω_3) and the excitation axis (ω_1) is retrieved by performing a Fourier transform along the first coherence time (t_1) giving a frequency-frequency correlated 2D map at a particular waiting time. The coherence time between the first two fields was scanned from -50 fs to 50 fs in steps of 0.2 fs and the waiting time was scanned from 0 to 420 fs with 4 fs step size. Depending on the ordering of the two pump fields, rephasing and nonrephasing signals are obtained. The absorptive 2D maps are obtained by summing up the phased real rephasing and nonrephasing signal.

2.4 Quantum Chemical Calculations: Density functional theory (DFT) was used to perform ground state optimization of the complexes in Gaussian 09 software package on adroit cluster in Princeton University.[12] Due to the large number of atoms in the $\mathbf{[1–N_2]^{2+}}$, phenyl rings at 4' position of the terpyridines were truncated to minimize the computation time for ground and excited state ogeommetry optimizations. Ground state optimization was intially perfomed with smaller basis set and eventually a larger basis set was chosen for final optimization. B3LYP functional with basis set 6-31G* for H, C, N, P, O, Cl and LANL2DZ for Mo was used in all the final calculations. Time-dependent DFT was used to perform single point energy calculation and final optimization of the two singlet electronically excited states. Natural Transition Orbital (NTO) analysis was performed to calculate the molecular orbitals involved in specific singlet and triplet transitions.

Figure S1. Natural transition orbital analysis of the three singlet transitions in $[\mathbf{1}–\mathbf{N_2}]^{2+}$ with maximum oscillator strength predicted by TDDFT calculations. The transitions are shown in increasing order of energy from left to right.

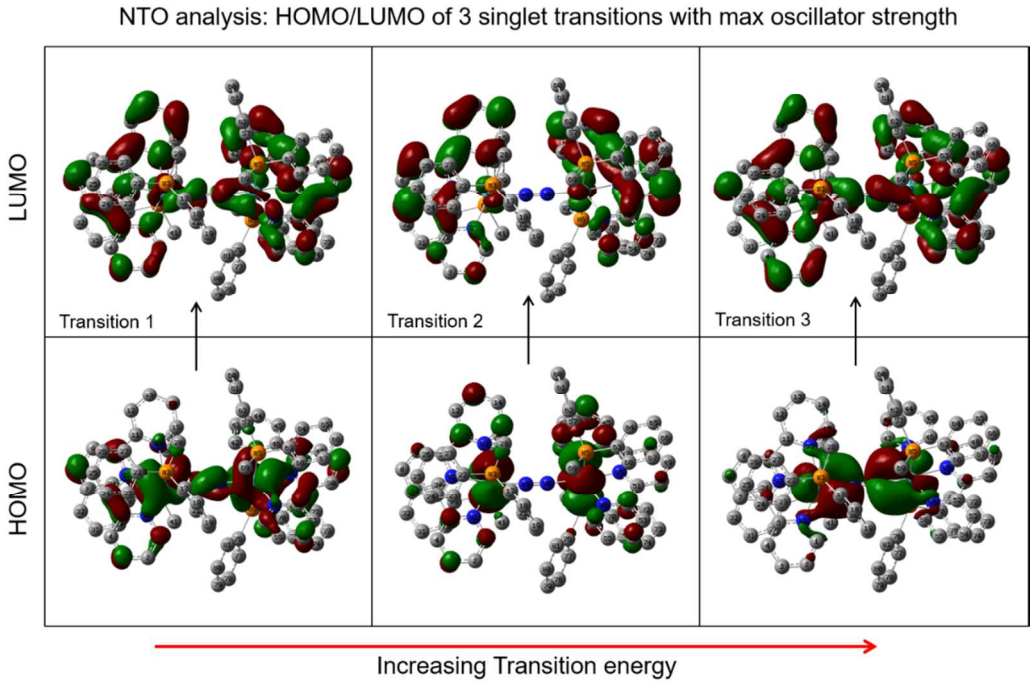

Figure S2. HOMO and LUMO molecular orbitals are calculated at TDDFT level of theory for the dinuclear metal complex in which the distance between the two nitrogen atoms of the bridge is elongated from 1.2Å (optimized bond length between the two nitrogen's) to 7Å to see the shift from delocalized nature of the molecular orbitals towards the localized molecular orbitals.

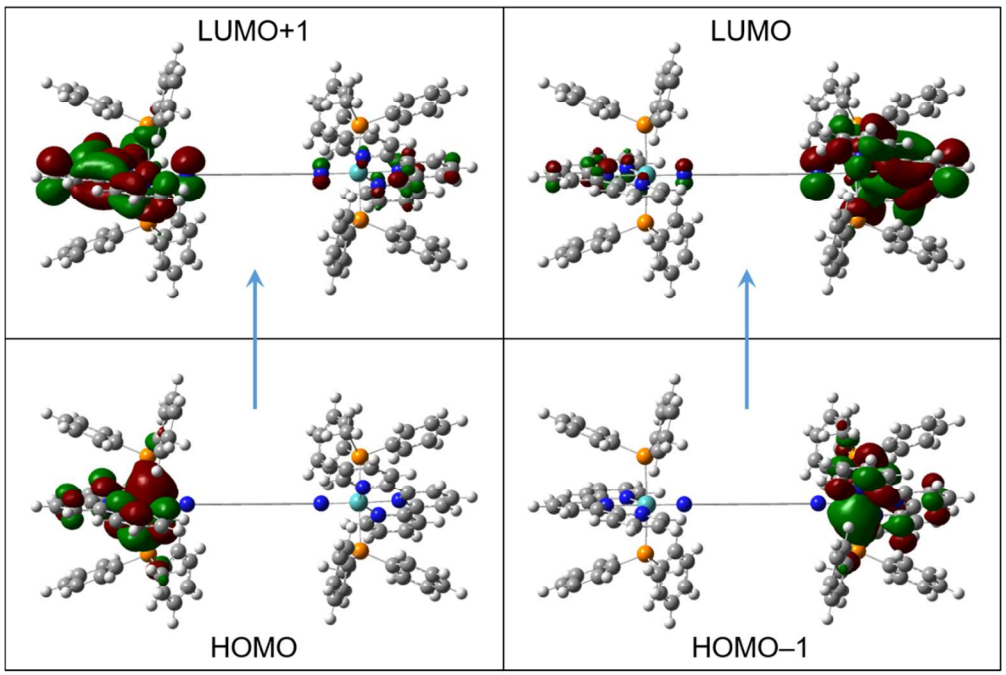

Figure S3: Time-resolved spectra at the indicated waiting times are shown for the metal complex for excitation wavelength of 520 nm in the visible (A) and near infra-red (B) probe region. (C) and (D) represent the decay associated spectra (DAS) obtained after the global analysis of the transient absorption data in the visible and near infra-red region respectively. (E) and (F) are the corresponding time-resolved spectra at indicated waiting times in the visible and near infra-red probe regions for 1150 nm excitation wavelength. (G) and (H) are the corresponding DAS spectra obtained after the global analysis of data for 1150 nm excitation. The plots with grey shaded background are DAS.

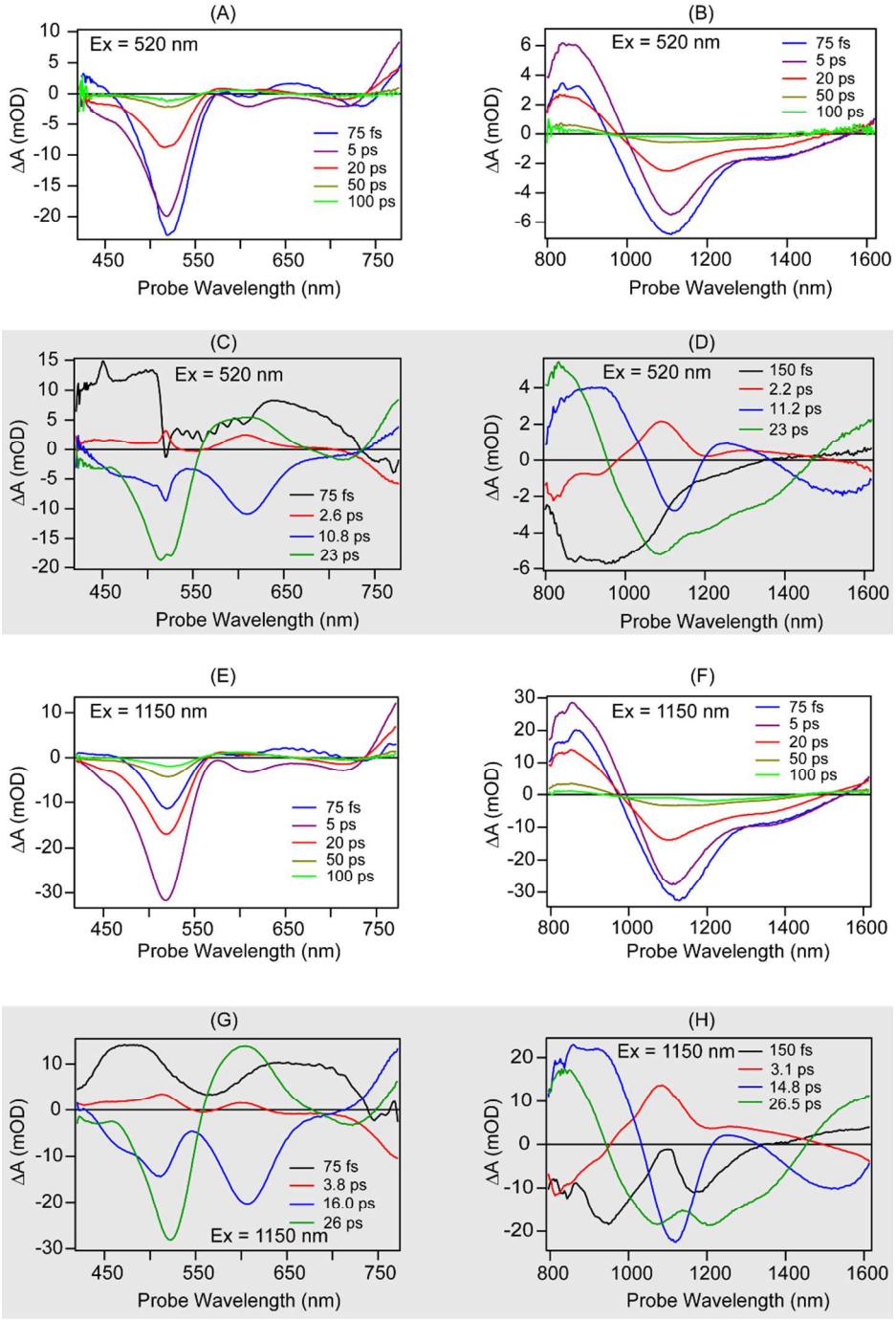

Table S1. Multiexponential fitting of the kinetic traces convoluted with a Gaussian function for the instrument response. The fitting parameters are presented as time constants in picoseconds with corresponding amplitudes in parenthesis. The kinetic trace at each wavelength was fitted with a minimum number of exponents needed to adequately represent the raw trace. Comparison of the fitting parameters at two different excitation wavelengths, 520 and 1150 nm is presented. The average lifetime of the kinetic traces was calculated by $\sum_i^n a_i \tau_i^2 / \sum_i^n a_i \tau_i$

Probe wavelength (nm)	Excitation at 520 nm		Excitation at 1150 nm	
	τ_i (a_i)	τ_{avg} (ps)	τ_i (a_i)	τ_{avg} (ps)
440	0.01(0.034) 0.25(0.0028) 2.18(0.001) 20.28(-0.0048)	19.67	0.07(0.008) 0.25(0.0013) 4.6(0.001) 21.98(-0.0051)	21.13
520	0.15(0.007) 20.3(-0.038)	20.27	0.11(0.008) 24.1(-0.038)	24.08
580	0.16(0.0036) 7.46(-0.0093) 4.47(0.0040) 39.0(0.0032)	25.70	0.07(0.0005) 7.05(-0.012) 4.94(0.008) 42.36(0.0027)	23.63
610	7.42(-0.013) 3.3(0.0053) 43.5(0.0025)	24.72	8.72(-0.011) 2.8(0.0037) 46.2(0.0025)	27.96
670	0.16(0.0086) 7.84(-0.0025)	7.34	0.088(0.0089) 8.92(-0.0024)	8.61
715	0.30(0.0014) 3.9(-0.0017) 23.07(-0.003)	21.28	 3.19(-0.00136) 24.8(-0.003)	23.61
770	2.62(-0.008) 19.9(0.016)	18.83	2.57(-0.0085) 21.1(0.017)	20.04
820	1.48(-0.008) 19.2(0.03)	18.84	2.21(-0.0096) 21.2(0.032)	20.62
850	0.057(0.188) 0.08(-0.18) 0.99(-0.006) 18.86(0.034)	18.00	0.013(0.245) 0.05(-0.087) 2.2(-0.007) 20.5(0.036)	19.93
900	0.38(-0.006) 16.99(0.029)	16.9	1.08(-0.0044) 19.1(0.029)	18.95
1000	0.12(-0.025) 4.97(0.009) 1.1(-0.003) 27.8(-0.0064)	22.60	0.067(-0.019) 5.53(0.0096) 1.48(-0.001) 27.9(-0.0068)	22.76
1100	0.087(-0.018) 2.29(0.0076) 19.7(-0.034)	19.22	0.016(-0.09) 2.47(0.01) 20.7(-0.035)	20.06
1300	0.01(-0.05) 2.22(0.0035) 27.7(-0.012)	27.08	0.01(-0.046) 2.63(0.0036) 28.3(-0.012)	27.57

Figure S4. Kinetics traces at 1100 nm probe wavelength are plotted at different pulse energies in nano-Joules of 1150 nm pump wavelength to rule out any two-photon absorption effects. Plot (a) shows the experimentally obtained kinetic traces for 10 nJ (red), 50 nJ (blue) and 300 nJ (black) pulse energies. Plot (b) shows the same kinetic traces but normalized to the same ΔA value to clearly see the effect of pulse energy on the dynamics. The independence of the dynamics on excitation pulse energies rules out two-photon absorption effects.

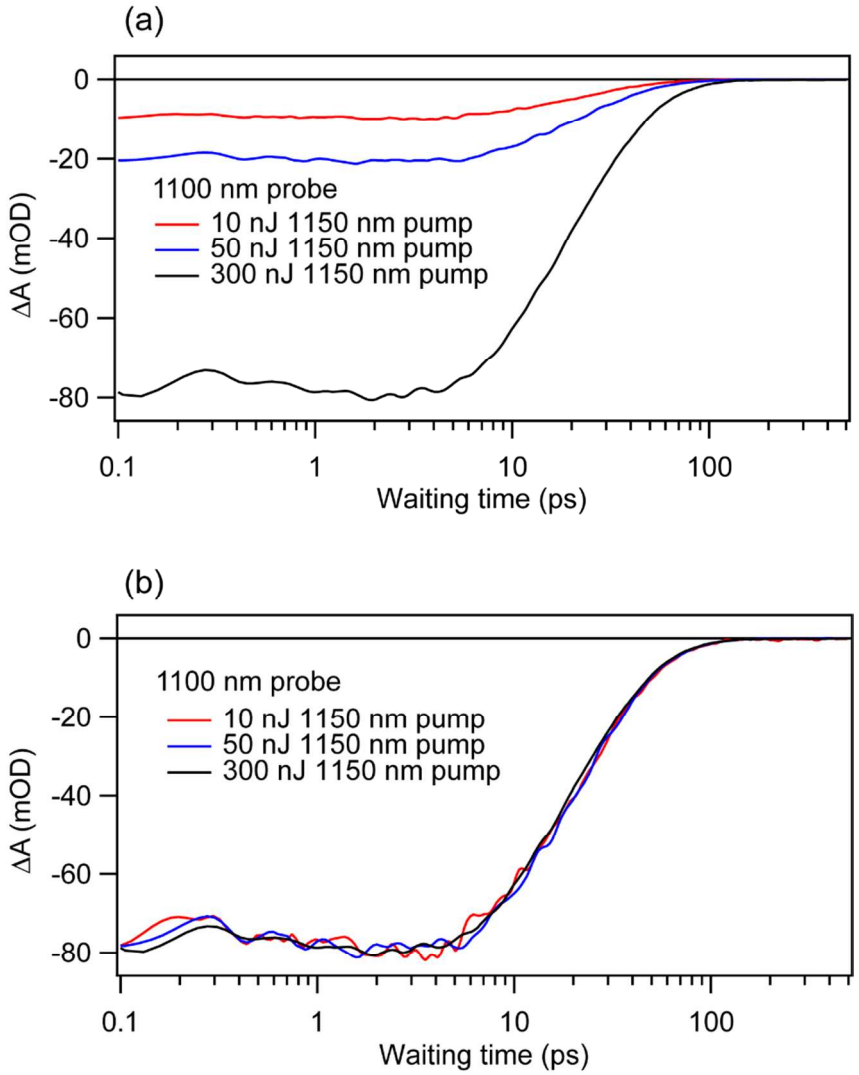

Figure S5. Transient absorption map of the mononuclear complex. The ground state completely recovers in less than 50 ps. A minimum of two global time-constants (2.3 ps and 13 ps) are required to adequately reproduce the experimental data. The signal on the positive side is excited state absorption and on the negative side is predominantly ground state bleach.

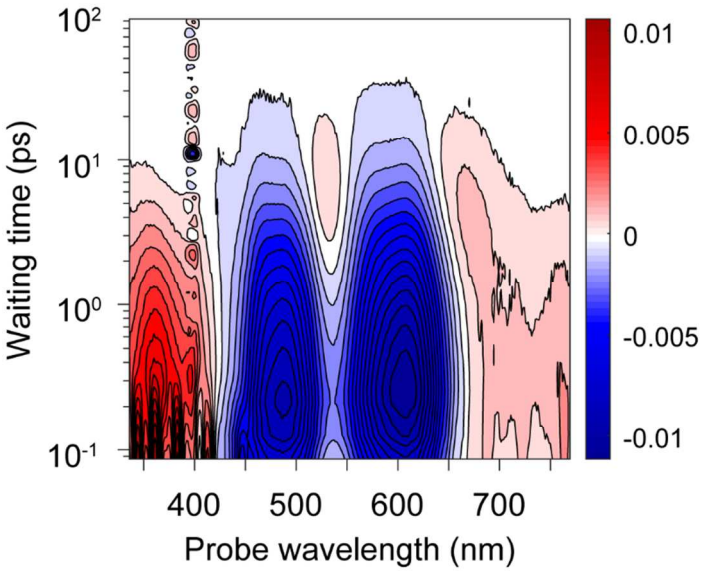

Figure S6. Double-sided Feynman diagrams drawn for a three-level system (one ground state and two electronically excited states) justifying the upper and lower cross-peaks observed in the 2D population maps.

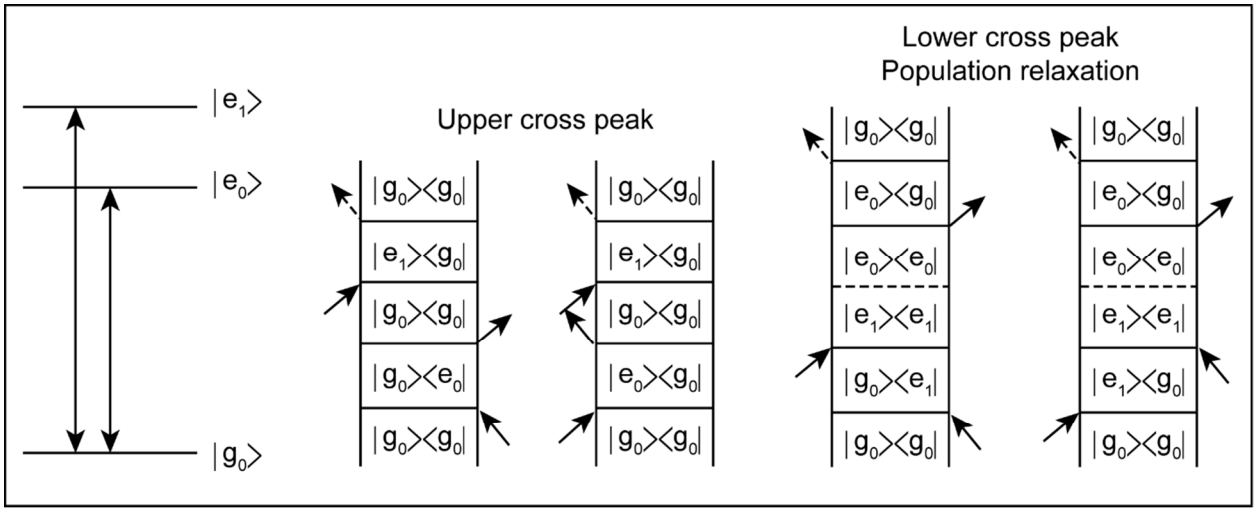

Figure S7. (a–c) represent the two-dimensional absorptive maps at 168, 280, and 440 fs waiting times obtained with pulse 2 shown in figure 5a. (d) shows the growth of the lower cross peak as a function of waiting time, indicative of population transfer from higher to the lower electronic state.

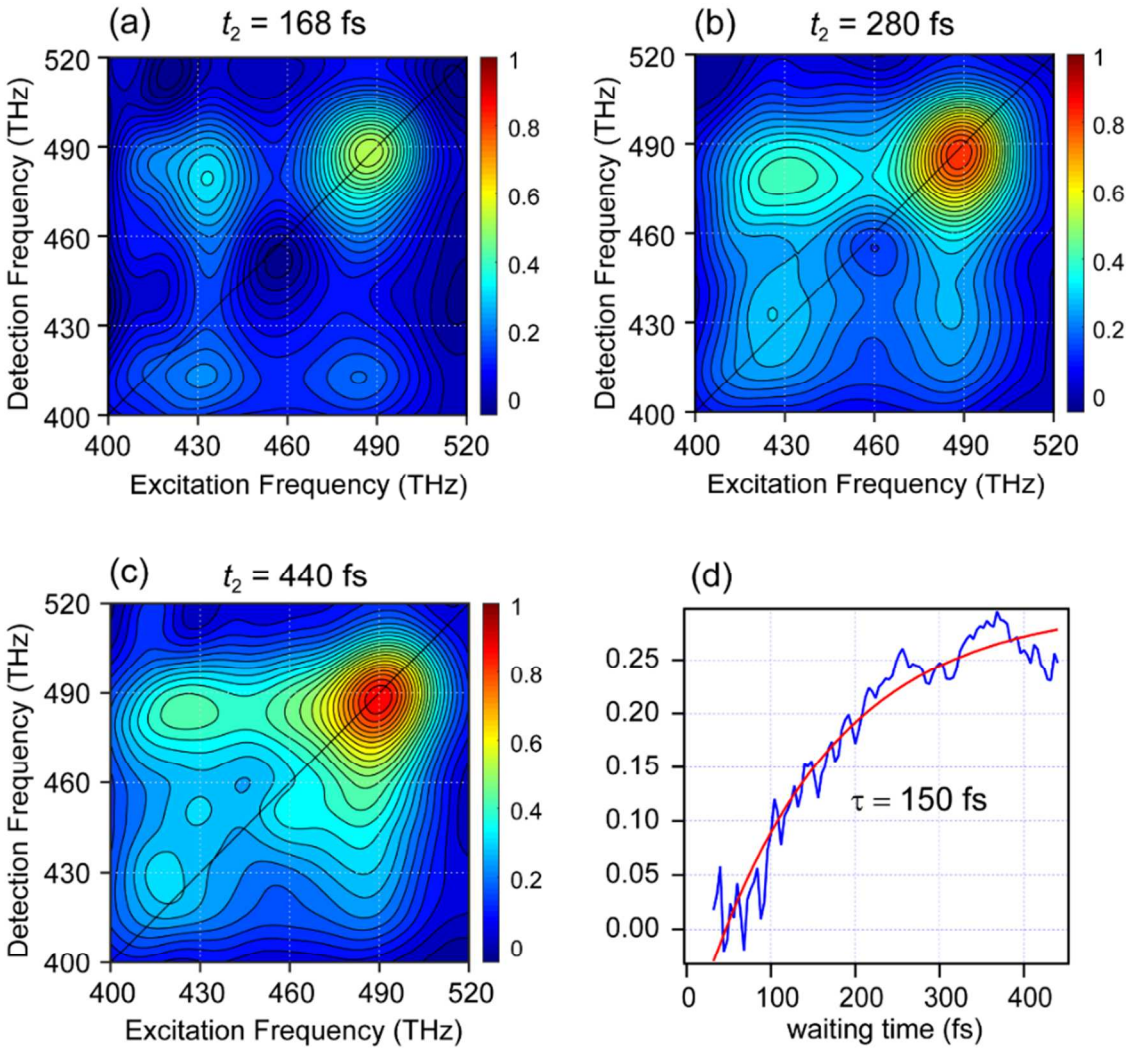

Figure S8. Natural transition orbital analysis of the three lowest triplet transitions predicted by TDDFT calculations. The transitions are shown in increasing order of energy from left to right.

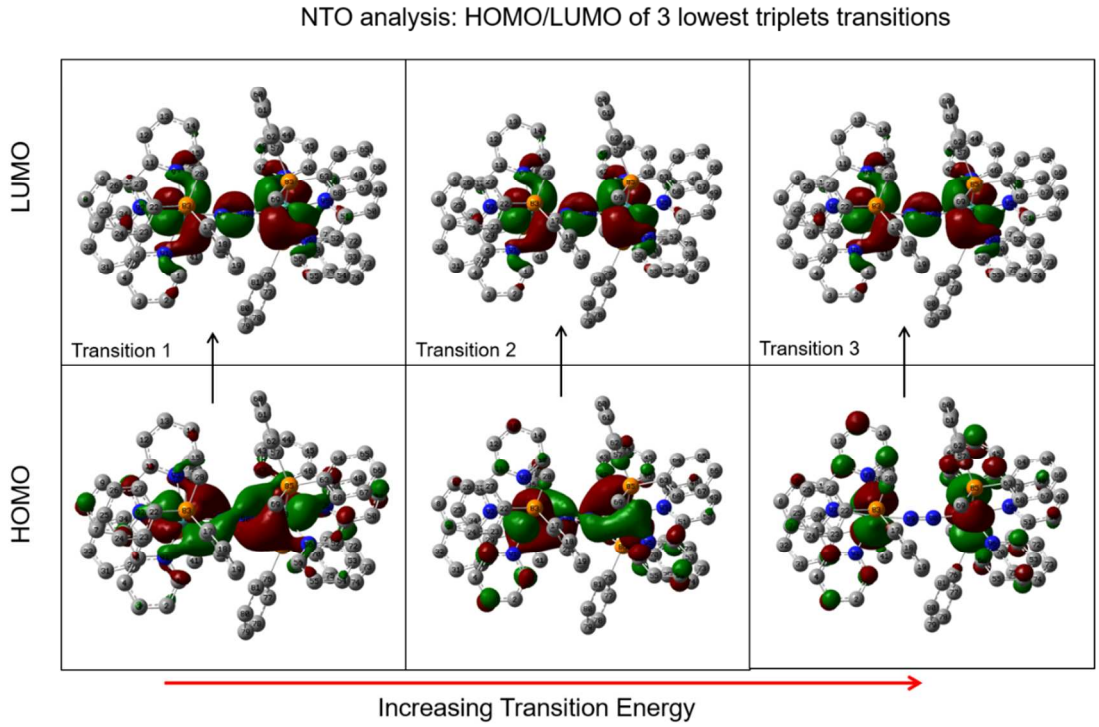

Figure S9. A schematic illustration of electronic localization occurring within 100 fs of electronic excitonic from the ground state to the electronically excited MLCT states. The absorption of a photon results in an excited electron delocalized over the two terpyridine ligands. However, due to the reduced electronic coupling (on behalf of large spatial separation) in the excited state, the electron localizes on either of the two terpyridines.

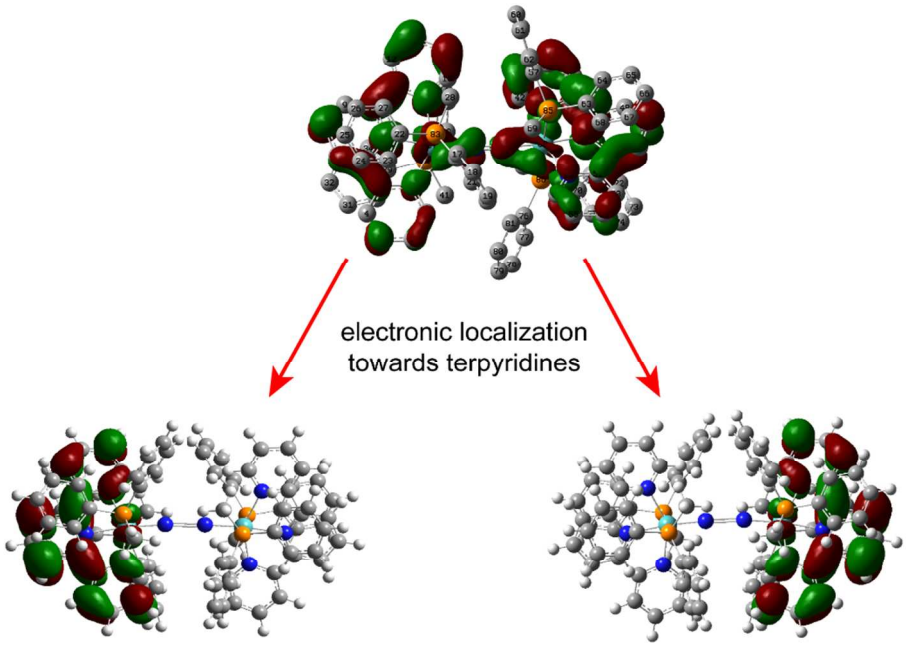

Figure S10. Structural relaxation in the excited state is confirmed by excited state optimization of the $[\mathbf{1–N_2}]^{2+}$ complex. (a) shows the angle between the two molybdenum-terpyridine planes along the Mo-N_2-Mo axis in the ground sate. (b) and (c) are the optimized structure of $[\mathbf{1–N_2}]^{2+}$ complex in two electronically excited states, where the angle between the Mo-terpyridine planes increases to 45° and 38°.

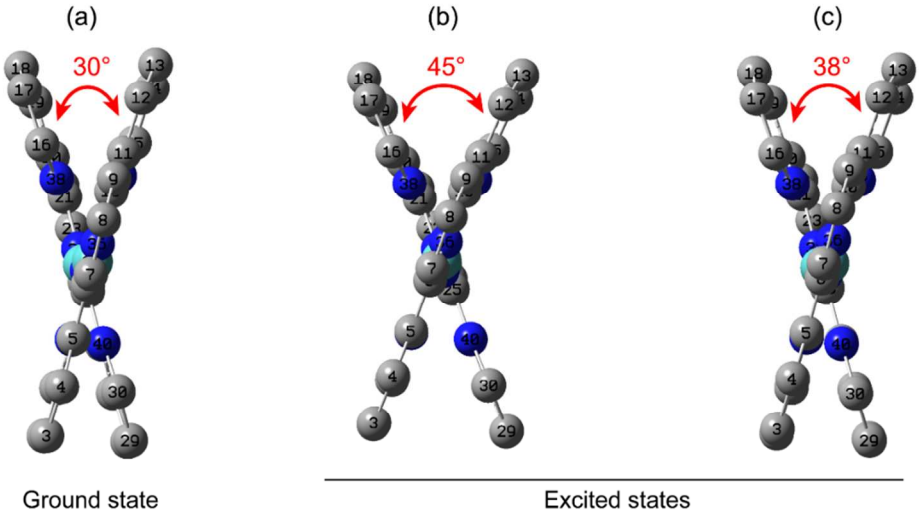

Figure S11. Kinetic traces shown for two representative probe wavelengths 715 nm (a) and 1100 nm (b) at room temperature (purple) and 77 K (red) upon excitation at 520 nm pump wavelength. 77 K measurements suggest a significant increase in the time-constants. Global analysis shows an increase of time-constants from 100 fs, 2-3 ps, 10-15 ps, 25 ps at room temperature to 100 fs, 6 ps, 100 ps, 610 ps at 77 K.

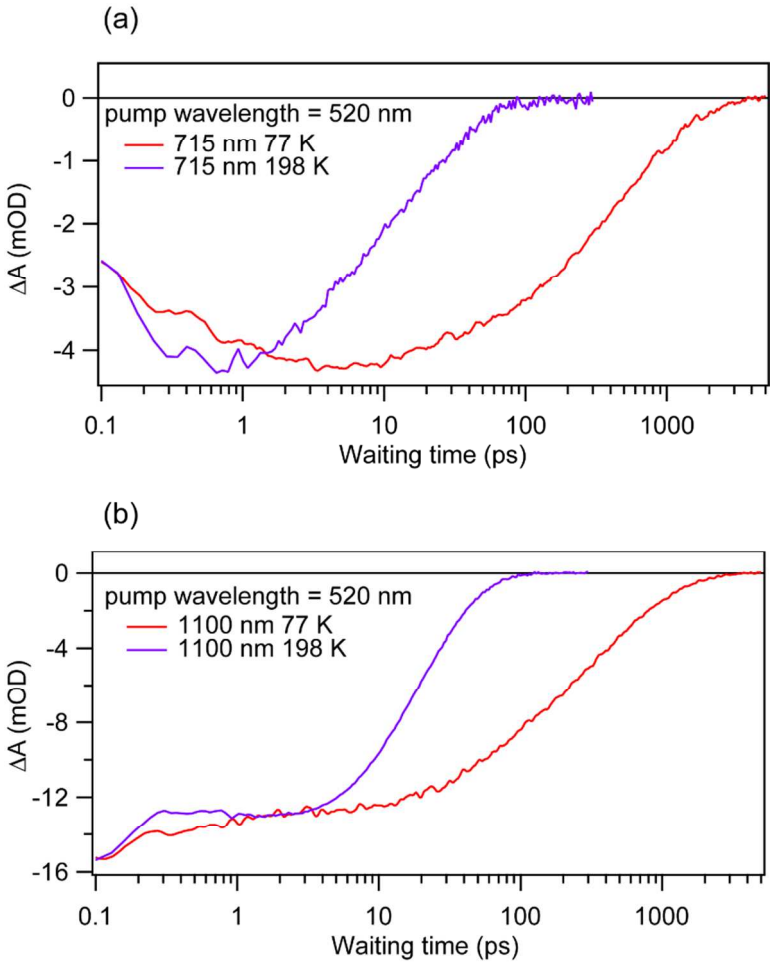

Figure S12. Natural Transition Orbitals (NTOs) of the singlet and triplet LUMOs showing migration of electron density from terpyridine ligands towards the dinitrogen substrate as the metal-complex non-radiatively transits from ^{1}MLCT to ^{3}MLCT state in about 2-3 ps.

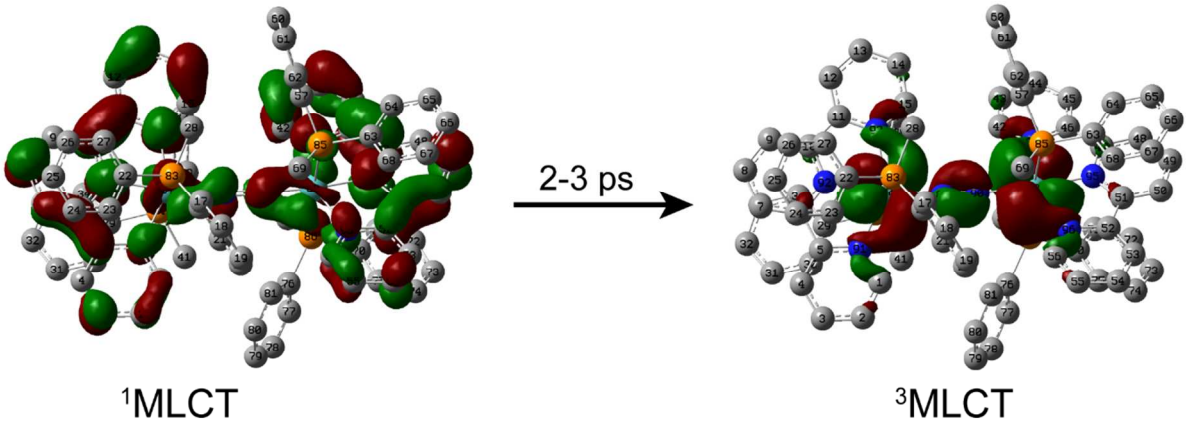

References

1. Pangborn, A. B.; Giardello, M. A.; Grubbs, R. H.; Rosen, R. K.; Timmers, F. J., *Organometallics* **1996,** *15* (5), 1518-1520.
2. Koch, M.; Myahkostupov, M.; Oblinsky, D. G.; Wang, S. W.; Garakyaraghi, S.; Castellano, F. N.; Scholes, G. D., *J. Am. Chem. Soc.* **2017,** *139* (15), 5530-5537.
3. McClure, S. D.; Turner, D. B.; Arpin, P. C.; Mirkovic, T.; Scholes, G. D., *J. Phys. Chem. B* **2014,** *118* (5), 1296-1308.
4. Turner, D. B.; Wilk, K. E.; Curmi, P. M. G.; Scholes, G. D., *Journal of Physical Chemistry Letters* **2011,** *2* (15), 1904-1911.
5. Anna, J. M.; Song, Y.; Dinshaw, R.; Scholes, G. D., *Pure Appl. Chem.* **2013,** *85* (7), 1307-1319.
6. Rafiq, S.; Scholes, G. D., *J. Phys. Chem. A* **2016,** *120* (34), 6792-6799.
7. Turner, D. B.; Dinshaw, R.; Lee, K.-K.; Belsley, M. S.; Wilk, K. E.; Curmi, P. M. G.; Scholes, G. D., *Phys. Chem. Chem. Phys.* **2012,** *14* (14).
8. Fork, R. L.; Cruz, C. H. B.; Becker, P. C.; Shank, C. V., *Opt. Lett.* **1987,** *12* (7), 483-485.
9. Trebino, R.; DeLong, K. W.; Fittinghoff, D. N.; Sweetser, J. N.; Krumbugel, M. A.; Richman, B. A.; Kane, D. J., *Rev. Sci. Instrum.* **1997,** *68* (9), 3277-3295.
10. Jonas, D. M., *Annu. Rev. Phys. Chem.* **2003,** *54*, 425-463.
11. Brixner, T.; Mancal, T.; Stiopkin, I. V.; Fleming, G. R., *J. Chem. Phys.* **2004,** *121* (9), 4221-4236.
12. Frisch, M. J.; Trucks, G. W.; Schlegel, H. B.; Scuseria, G. E.; Robb, M. A.; Cheeseman, J. R.; Scalmani, G.; Barone, V.; Petersson, G. A.; Nakatsuji, H.; Li, X.; Caricato, M.; Marenich, A.; Bloino, J.; Janesko, B. G.; Gomperts, R.; Mennucci, B.; Hratchian, H. P.; Ortiz, J. V.; Izmaylov, A. F.; Sonnenberg, J. L.; Williams-Young, D.; F. Ding, F. L.; F. Egidi, J. G.; B. Peng, A. P.; Henderson, T.; Ranasinghe, D.; Zakrzewski, V. G.; Gao, J.; Rega, N.; Zheng, G., *Gaussian 09, Revision C.01*. Gaussian, Inc., Wallingford CT, 2010.